V.R.3 Water Transport Exploratory Studies

Rod Borup[1] (Primary Contact),
Rangachary Mukundan[1], John Davey[1],
David Wood[1], Tom Springer[1], Yu Seung Kim[1],
Jacob Spendelow[1], Tommy Rockward[1],
Bryan Pivovar[1], Muhammad Arif[2],
David Jacobson[2], Daniel Hussey[2], Ken Chen[3],
Karren More[4], Peter Wilde[5], Tom Zawodzinski[6],
Vladimir Gurau[6], Will Johnson[7],
Simon Cleghorn[7]

[1]Los Alamos National Laboratory
MS J579, P.O. Box 1663
Los Alamos, NM 87545
Phone: (505) 667-2823; Fax: (505) 665-9507
E-mail: Borup@lanl.gov

DOE Technology Development Manager:
Tim Armstrong
Phone: (865) 574-7996; Fax: (865) 241-0112
E-mail: armstrongt@ornl.gov

Technical Advisor: John Kopasz
Phone: (630) 252-7531; Fax: (630) 972-4405
E-mail: kopasz@cmt.anl.gov

Subcontractors:
[2] National Institute of Standards and Technology (NIST), Gaithersburg, MD
[3] Sandia National Laboratories, Albuquerque, NM
[4] Oak Ridge National Laboratory, Oak Ridge, TN
[5] SGL Technologies GmbH, 86405 Meitingen, Germany
[6] Case Western Reserve University, Cleveland, OH
[7] W.L. Gore and Associates, Elkton, MD

Start Date: March 2007
Project End Date: Project continuation and direction determined annually by DOE

Objectives

- Develop understanding of water transport in proton exchange membrane (PEM) fuel cells.
  - Non-design-specific (as possible)
- Evaluate structural and surface properties of materials affecting water transport and performance.
- Develop (enable) new components and operating methods.
- Accurately model water transport within the fuel cell.
- Develop a better understanding of the effects of freeze/thaw cycles and operation.
- Present and publish results.

Technical Barriers

This project addresses the following technical barriers from the Fuel Cells section of the Hydrogen, Fuel Cells and Infrastructure Technologies Program Multi-Year Research, Development and Demonstration Plan:

(D) Water Transport within the Stack

Technical Targets

- Energy efficiency (65% at 25% rated power, 55% at 100% rated power)
- Power density (2,000 Watt/l)
- Specific power (2,000 Watt/kg)
- Cost ($25/kWe)
- Start up time to 50% power (30 seconds from -20°C, 5 seconds from 20°C)
- Freeze Start Operation (Unassisted start from -40°C)
- Durability with cycling: 5,000 hrs

Accomplishments

- Direct water imaging at NIST using neutron radiography.
  - High resolution (~25 μm) cross-section cell design
    - Cross-section view
  - Low resolution (150 μm) imaging
    - Imaging of entire 50 cm^2 flowfield area
  - Imaging of water/ice in fuel cells operated at sub-freezing temperatures
- Freeze/thaw examination of PEM fuel cells.
  - Comparison of backing layers on durability
- Testing, evaluation and characterization of gas diffusion layers (GDLs).
  - Varying GDL materials and operating conditions
    - GDL substrate and micro porous layer (MPL) polytetrafluoroethylene (PTFE) loading
  - Hydrophobicity characterization
  - Microscopic characterization of hydrophobic coating
  - Elemental compositional characterization
- Modeling of mass transport losses.
  - Delineation of mass transport loss from infrared (IR), kinetics, etc.
- Modeling of water transport and removal.

– Elucidating water-droplet detachment from the GDL/channel interface

Introduction

Efficient fuel cell performance requires effective water management. While this statement sounds simple, the combinations of materials used, their durability, and the operating conditions under which fuel cells run, make accomplishing efficient water management within a practical fuel cell system one of the primary challenges in developing commercially viable systems. Specific components such as the PEMs and electrode layers require sufficient water to be present in order to allow adequate proton conductivity. Conversely, excess water within the system leads to mass transfer losses and can require additional balance of plant costs (extra energy or weight for increased humidification). The range of conditions under which the system is required to operate makes meeting all these requirements at the same time even more difficult. The conditional extremes provide the biggest challenges: maintaining hydration under hot/dry conditions and preventing flooding/dealing with ice formation under cold/wet conditions. Perhaps the most challenging of these conditions is subfreezing temperatures. In order to compete with internal combustion engines, the DOE has stated goals for fuel cell survivability (-40°C), start-up time (30 seconds to 50% rated power from -20°C), and energy (5 MJ) under subfreezing conditions. In order to address these challenges there is a need for increased understanding of water transport and phase change within fuel cell components. This requires that the structure and properties of fuel cell materials be fully understood. The materials ultimately employed will need durability under normal and transient operations while allowing effective water management under any environmentally-relevant condition.

To achieve a deeper understanding of water transport and performance issues associated with water management, a multi-institutional and multi-disciplinary team with significant experience investigating these phenomena has been assembled. This team is headed by Los Alamos National Laboratory (LANL) and includes two other National Laboratories (Sandia [SNL] and Oak Ridge [ORNL]), a university (Case Western Reserve University [CWRU]), a membrane electrode assembly (MEA) supplier (W.L. Gore), a GDL supplier (SGL Carbon Group), and the National Institute of Standards and Technology (NIST).

This report describes our FY 2007 technical progress in characterizing and quantifying the durability of fuel cell components and their degradation mechanisms to support the DOE Hydrogen and Fuel Cell Infrastructure Technologies Program.

Approach

Our approach to understanding water transport within fuel cells is structured in three areas: fuel cell studies, characterization of component water transport properties, and modeling of water transport. These areas have aspects that can be considered free-standing, but each benefit greatly from work performed in the other areas. The modeling studies tie together what is learned during component characterization and allow better interpretation of the fuel cell studies. This approach and our team give us the greatest chance to increase the understanding of water transport in fuel cells and to develop and employ materials that will overcome water-related limitations in fuel cell systems.

To help understand the effect of components and operational conditions, we examine water transport in operating fuel cells, measure the water content and location of water during operation, and make water balance measurements. Segmented cell operation of fuel cells is being conducted, evaluating the high frequency resistance (HFR) of the cell as a function of channel inlet distance, inlet relative humidity (RH), current density, and component variation. Neutron imaging is being utilized to visualize *in situ* water transport under reasonable steady-state and transient operating conditions and watch ice formation and locate frozen water in freezing cells (both under operation and during shut-down conditions). We also characterize the properties of the GDL before and after various fuel cell operations in order to quantify durability issues associated with water transport. Lastly, we develop analytical and multi-dimensional numerical models to elucidate the key phenomena of water transport and removal within GDLs and channels, and at the GDL/channel interfaces.

Results

Vary GDL Hydrophobicity

Many components of PEM fuel cells contribute to the overall water management during operation. However, the purpose of the GDL is primarily to enhance mass transport within the fuel cell; specifically removal and distribution of water coupled with reactant gas feed. To help evaluate the effect of GDL hydrophobicity on fuel cell performance, we varied the coating of GDL substrates and MPLs and tested as a function of inlet RH and current density. The water content variation utilizing these GDL hydrophobic treatments were also imaged via neutron radiography. Three different hydrophobic treatment variations were

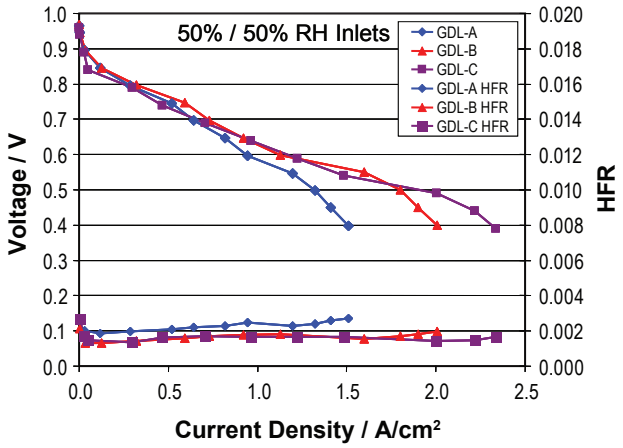

FIGURE 1. Voltage/current density curves of GDLs with varying PTFE coatings at inlet RHs of 50%/50%. GDL A had a substrate PTFE loading of 5% and MPL loading of 23%; GDL B 5% substrate and 10% MPL; GDL C 20% substrate and 10% MPL. Operating conditions: 172 kPa, 1.1/2.0 stoichiometry, 80°C cell temperature; MEA catalyst loading was 0.2/0.4 Pt/cm^2.

used: GDL A had a substrate PTFE loading of 5% and MPL loading of 23%, GDL B 5% substrate and 10% MPL, GDL C 20% substrate and 10% MPL. Figure 1 shows polarization curves of three cells utilizing these GDLs with an inlet RH of 50% for both anode and cathode. The performance of the these cells was similar at low current densities, but as the current density increased, discrepancies in performance increased, with the best performance being from the GDL with PTFE loading of 20% substrate and 10% MPL. The performance trend between the GDL materials held true for 50%, 75% and 100% cathode inlet RH. In addition, the HFR shows that the lowest performing cell also has the highest resistance at all the current densities and inlet cathode RHs studied. This examination indicates that lower MPL PTFE loading leads to improved fuel cell performance under these operating conditions. Note that the GDL on the anode side of the cell was kept constant, and was GDL A. Only the cathode GDL material was varied.

Full AC impedance spectra were taken for these cells with varying hydrophobic treatments. The AC impedance spectra were modeled using an equivalent circuit to separate charge transfer resistance from mass transport resistance. The HFR decreases with increasing current and decreases with increasing RH regardless of the GDL treatment, however is greater for the GDL with 23% PTFE in MPL. The charge transfer resistance also decreases with increasing RH and with increasing current, and is also greatest for the GDL with 23% PTFE in MPL. Mass transfer resistance increases with increasing RH and increasing current, and is also greatest for GDL with 23% PTFE in MPL.

Neutron imaging of cells utilizing varying degrees of hydrophobic treatments were conducted to help elucidate the effect of the GDL on water content inside the operating cell. Neutron radiography is a powerful tool that can be used to visualize (*in situ*) the water content in an operating fuel cell [1,2]. Previously reported neutron imaging experiments have been performed using an amorphous silicon detector with a resolution of approximately 150 μm. Here we report results from a higher resolution 25 μm micro channel plate (MCP) detector. The use of the higher resolution detector in combination with a specially designed 2.25 cm^2 active area cell enabled the direct imaging of water in the GDLs and flow fields independently. Comparing Figures 2a and 2b shows the effect of current density and cathode inlet RH on the water profile within the fuel cell. There is more water (black = no water; blue/white = more water) accumulating near the outlets than near the inlets and the amount of this water increases with increasing current density and cathode inlet RH. The water near the outlet is more concentrated in the cathode GDL, especially the GDL above the land area. This is consistent with the creation of water at the cathode and its removal by the gas flow in the channels. The water created above the land area needs to diffuse out laterally to the channel before it can be removed through the flow fields. The PTFE content in the microporous layer of the GDL was also varied from 23% by weight to 10% by weight and its influence on the water profile is seen by comparing Figures 2c and 2d. The MPL with the 23% by weight PTFE loading showed significantly greater water accumulation under identical conditions of operation. Moreover, this cell also showed significant water in the anode GDL (near the outlet) due to back diffusion. These results can be directly correlated to the performance of standard 50 cm^2 cells using these two GDLs. The GDL with the lower PTFE loading in the MPL showed better performance at high current densities (see Figure 1) associated with a lower mass transport resistance as determined by AC impedance analysis. Therefore, neutron imaging can be used as tool to not only optimize cell designs but also to optimize the various fuel cell components that affect water transport.

By integrating the water content from the high resolution images such as those shown in Figure 2, the water concentration can be observed by location within the cell; i.e. in the GDL above the land vs. in the GDL above the channel. The relative water content in a fixed portion of the anode and cathode GDL at various cell locations is shown in Figure 3 for a 2.25 cm^2 cell operated at 1.0 A/cm^2 and 100% inlet RH anode/cathode. The cell has a single serptentine flow field with 11 channels and 12 lands perpendicular to the imaging view. The water content increases as the gases progress down the flowfield, with the water content above the flowfield lands being greater than that above

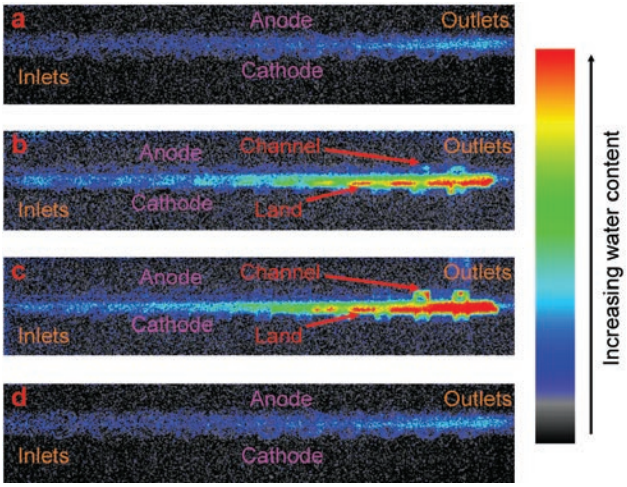

FIGURE 2. High resolution neutron imaging of 2.25 cm^2 active area cells (a) 5% PTFE GDL substrate and 10% PTFE MPL at 0.2 A/cm^2, cathode: 50% RH, anode: 50% RH; (b): 1.4 A/cm^2, anode: 50% RH, cathode: 100% RH; (c) 23% PTFE in the MPL and 5% PTFE in the substrate operated at 0.2 A/cm^2, 50% RH; (d) 10% PTFE in the MPL and 5% PTFE in the substrate 50% RH. All cells were operated at 1.1/2.0 anode/cathode stoichiometry and 172 kPa.

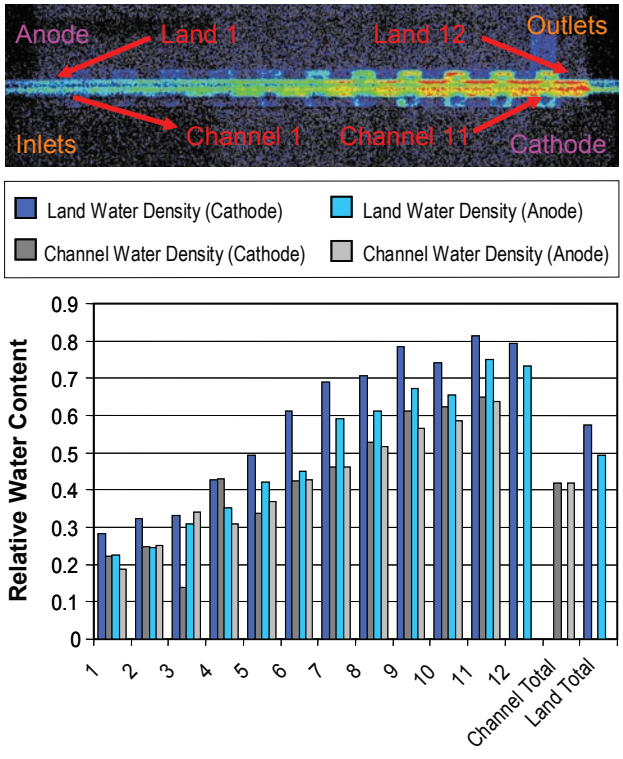

FIGURE 3. High resolution neutron image and relative water content of anode/cathode lands and channels. Dark blue: cathode land water density; light blue: anode land water density; dark grey: cathode channel water density; and light grey: anode channel water density. Cell was 2.25 cm^2 active area with single serpentine, 1.0 A/cm^2, 100% inlet RH for anode and cathode.

the channels. In addition, the water content on the cathode side is greater than that of the anode, which would be expected, however most of the difference in water content between anode and cathode seems to occur above the land area. The overall water content above the channels seems similar in comparing anode to cathode.

PEM Fuel Cells at Sub-Freezing Temperatures

We have previously characterized the performance of both cloth (E-tek) and SGL paper GDLs and reported that the paper GDLs show lower tolerance to sub-freezing temperatures [3]. Here, we report accelerated testing of GDLs under sub-freezing conditions that confirms our initial results. The cells were initially tested at 80°C with fully humidified H_2 and air streams at the anode and cathode. After testing, the gases were shutdown and the cells were capped and cooled to retain the maximum amount of water. The cells were then subjected to freezing at -40°C using both slow (4 hours to -40°C) and fast (<1 hour to -40°C) cooling. The performance of the cloth GDL shows little degradation during 100 freeze/thaw cycles down to -40°C. Figure 4 illustrates the performance of a paper GDL under the same conditions showing large degradation at the high current densities (>0.5 A/cm^2). This degradation was accompanied by an increase in the low frequency resistance (mass transport) of the cells. The cells that were fast cooled also showed similar degradation.

A fuel cell with cooling loops machined in the end plates was designed in order to study the start-up behavior of single 50 cm^2 cells. The cells were

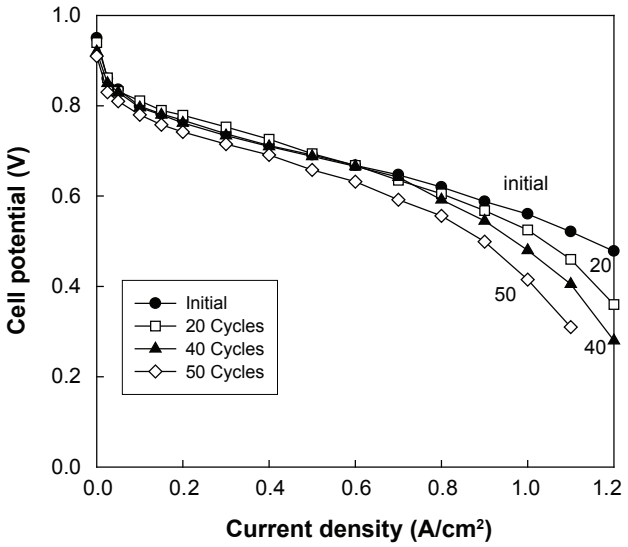

FIGURE 4. Performance of a Fuel Cell with Paper GDL after 100 Freeze/Thaw Cycles to -40°C

first operated at 80°C at 100% RH and 30 psi back pressure. The cells were then shut down (open circuit) and dried using a N_2 purge (1,000 cc/min at the anode and 5,000 cc/min at the cathode) for <3 minutes and cooled down to -10°C. Dry H_2 and dry air were then introduced into the anode and cathode of the cells at -10°C (isothermal) and their performance at a constant voltage of 0.6 V was monitored. The current initially spiked and decayed to a steady-state value. During this decay both cyclic voltammograms and AC impedance spectra were obtained. These revealed that although there was not much change in the active catalyst surface area (H_2 adsorption peak), the mass transport resistance progressively increased (low frequency resistance) due to ice formation. The exact location of the ice formation is not known at this time. However, when the cells were heated back up to 80°C, they recovered their initial performance. There was little performance decay observable at 80°C after three such isothermal operations at -10°C.

To further elucidate operation of fuel cells under subfreezing conditions, neutron images were taken under these conditions. Figure 5 shows neutron imaging of a fuel cell during operation at subfreezing temperatures (-10°C). This image shows the entire flowfield of a 50 cm^2 fuel cell. The cell was initially operated at 1.4 A/cm^2 and 100% RH at the cathode and anode and then purged dry at 80°C before cooling to -10°C. The cell was then operated at a constant voltage of 0.5 V flowing dry H_2 at 300 cc/min and dry air at 500 cc/min at the anode and cathode respectively. Figure 5a shows the average water content during the initial 1.6 minutes of operation. Figure 5b shows the final 1.6 minute average water content after 15 minutes of operation. As these images were taken at subfreezing conditions, the water which is formed from the electrochemical reaction likely stays close to where it is produced and freezes. These images show the gradual build-up of water/ice during operation, with the greatest amount of water (ice) being formed towards the top and outlet edge of the flowfield. As the operation of the cell is at -10°C, it is likely that the water produced during operation stays within the cell as ice. Figure 5c shows the water content of the cell at subfreezing conditions over-layed with cumulative current density. The water content by neutron imaging appears to show a direct correlation with the cumulative current density, which shows that the product water does stay within the cell at these operating temperatures, and neutron imaging is effective at monitoring the solid water phase.

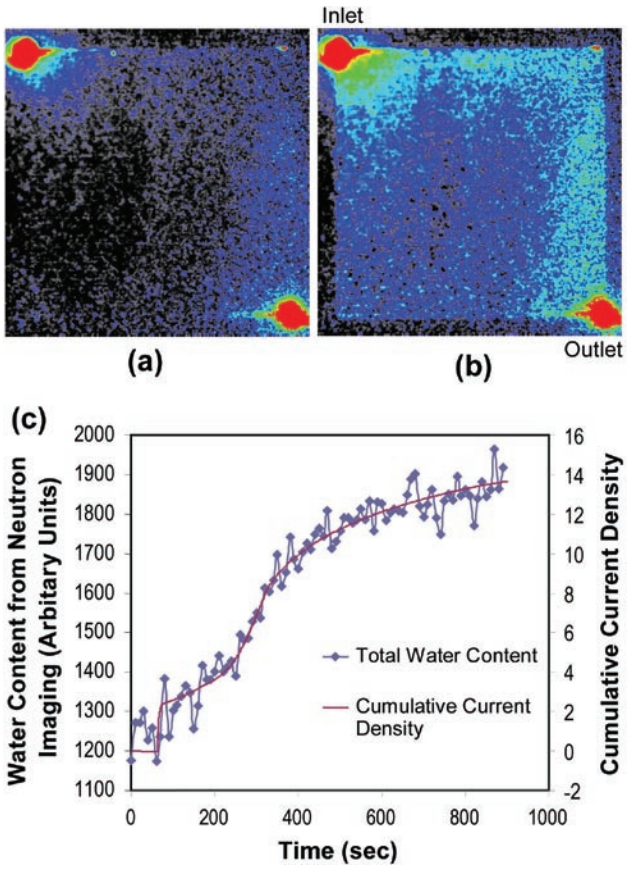

FIGURE 5. Neutron imaging during start-up under subfreezing conditions (-10°C). Cell was initially purged dry, then fuel cell operation initiated at a constant voltage of 0.5 V. 5a is the average water content during the initial 1.6 minutes of operation. 5b is the final 1.6 minute average water content after 15 minutes of operation. 5c shows the integrated overall water content and the integrated cumulative current density.

Model Prediction of Onset of Water-Droplet Detachment

Water droplet detachment from the GDL/channel interface is a key mechanism for liquid-water removal in PEM fuel cells. Elucidating water-droplet detachment from GDL/channel interface and being able to predict the critical air-flow velocity required to detach droplets helps provide critical design and operational guidelines. A model for predicting the critical air-flow velocity, U_c has been developed by making a force balance on water droplets at the onset of detachment. This model (Equation 1) is based on the force balance between viscous shearing/pressure drag that tends to detach the droplet and surface tension that tends to hold the droplet in place. We account for the viscous shearing that dominates in the flow regime with low Reynolds numbers as well as the pressure drag arising from inertia effects (i.e., when the Reynolds number is relatively high). This assumes that the pressure drag due to inertial effects dominates the droplet detachment.

Solving for the critical air-flow velocity, U_c, yields:

$$U_c = \left[\frac{H_c}{\rho\,\mu}\right]^{1/3}\left[\frac{\pi\gamma\sin^2\theta_s\sin\frac{1}{2}(\theta_a-\theta_r)}{5(\theta_s-\sin\theta_s\cos\theta_s)d}\right]^{2/3} \quad (1)$$

where: d is the water droplet diameter; H_C is the channel height; ρ and μ are density and viscosity, respectively, of the flowing air; γ is the surface tension, θ_s denotes the static contact angle in radians; θ_a and θ_r are the advancing and receding contact angles, respectively.

Equation 1 shows that the critical velocity varies inversely (to the 2/3 power) with the water-droplet size. Furthermore, Equation 1 indicates that making the GDL surface more hydrophobic (i.e., increasing θ_s) and decreasing contact-angle hysteresis (i.e., decreasing $\theta_a - \theta_r$) reduce the critical velocity.

To help assess the validity of our model, experimental data reported by Zhang et al. [4] and Theodorakakos et al. [5] are compared with the model prediction as shown in Figure 6. The channel height used by Theodorakakos et al. work is 2.7 mm whereas that used by Zhang et al. is 0.5 mm. In computing the model prediction as shown in Figure 6, the following static contact angle and contact-angle hysteresis values were used: i) $\theta_s = 130°$, $\Delta\theta$ ($\equiv\theta_a - \theta_r$) = 50° for Theodorakakos et al. (2006) with carbon paper GDL; ii) $\theta_s = 145°$, $\Delta\theta$ ($\equiv\theta_a - \theta_r$) = 60° for Theodorakakos et al. (2006) with carbon cloth GDL; and iii) $\theta_s = 150°$, $\Delta\theta$ ($\equiv\theta_a - \theta_r$) = 15° for Zhang et al. (2006) with carbon paper GDL. As seen in Figure 6, agreements between experimental data and model prediction for the three cases are good using the static contact angle and contact-angle hysteresis values reported above. Notice that the contact-angle hysteresis value used for Zhang et al. work is considerably lower than that used for Theodorakakos et al. work; this can be attributed to the fact that the Zhang et al. data were obtained using an operating fuel cell (in which the GDL surface may have been wetted by the condensation of water vapor) whereas the Theodorakakos et al. data were obtained using a simulated flow channel with water droplets of varying sizes being placed on the GDL surface (in this case, there existed no complication of water-vapor condensation). Note that the contact-angle hysteresis value, $\theta_a - \theta_r$, is a key parameter in our model, which can contain significant uncertainty.

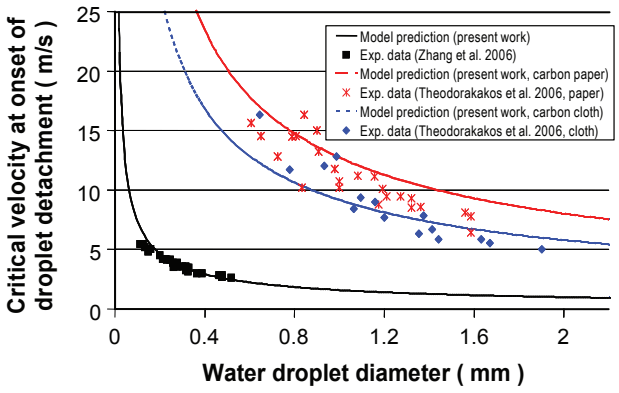

FIGURE 6. Effects of GDL Properties on Water-Droplet Detachment: Sample Prediction and Model Validation

Conclusions

- Changing mass transport properties during fuel cell operation lead to decreased performance:
  - GDL material properties change during aging.
  - Mass transport decay correlates to hydrophobicity loss of GDL.
  - Fluorine redistributes in GDL during start/stop operation.
- PTFE loading in GDL and MPL affects water transport:
  - Greater mass transfer resistance for GDL with 23% PTFE in MPL.
  - Substrate PTFE content does not have major role in determining water content.
- Neutron imaging shows water distribution of flow field and of MEA cross-section:
  - Water build-up in flow field of both anode and cathode at constant stoichiometric operation.
  - More water accumulation in GDL under land area when compared to the GDL under flow channel area.
- Subfreezing operation:
  - Operation at subfreezing temperatures builds up water (ice) in the cell.
  - Ice buildup directly correlates with current density (via neutron imaging).
  - Neutron imaging is effective at monitoring the solid water phase.
  - Significant mass transport problem after 80 freeze-thaw cycles to -40°C for the paper GDL.
- Modeling predicts:
  - More hydrophobic GDL materials reduce the critical velocity required to detach water droplets.
  - Decreasing contact-angle hysteresis (e.g., by reducing GDL surface roughness) enhances droplet removal.

Future Directions

- Water balance measurements:
  - Transient inlet RH measurements.
- NIST neutron imaging:
  - Hydrophillic catalysts.
  - Freeze operation.
- Freeze measurement:
  - *In situ* monitoring of ice formation.

- Two-phase model development:
  - Analyzing flow mal-distribution among PEM fuel cell channels.
  - Sub-model of liquid-water removal due to evaporation at the liquid/gas interface.
  - Develop a multi-dimensional (quasi-3D) model of water transport and removal.
  - Incorporate sub-models of liquid-water removal via droplet detachment and evaporation.

FY 2007 Publications/Presentations

1. R. Mukundan, J. R. Davey, T. Rockward, J. S. Spendelow, D. S. Hussey, D. L. Jacobson, M. Arif, and R. L. Borup, **Imaging of Water Profiles in PEM Fuel Cells using Neutron Radiography: Effect of Operating Conditions and GDL Composition**, submitted to The Electrochemistry Society.

2. R. Mukundan, Y. S. Kim, T. Rockward, R. Borup and B. Pivovar, **Performance of PEM Fuel Cells at Sub-Freezing Temperatures,** submitted to The Electrochemistry Society.

3. R. L. Borup, M. Rangachary, J. R Davey, Y. S. Kim, J. Spendelow, T. Rockward, M. Arif, D. Jacobson and D. Hussey, **PEM Fuel Cell Water Transport Exploratory Studies,** submitted to the Fuel Cell Seminar.

4. R. Borup, R. Mukundan, J. Davey, D. Wood, T. Springer, Y. S. Kim, J. Spendelow, T. Rockward, B. Pivovar, M. Arif, D. Jacobson, D. Hussey, K. Chen, K. More, P. Wilde, T. Zawodzinski, V. Gurau, W. Johnson, S. Cleghorn, **Water Transport Exploratory Studies,** Presented at the 2007 DOE EERE Hydrogen, Fuel Cells & Infrastructure Technologies Program Review, Washington, D.C., May 14–19, 2007.

5. R. Borup, R. Mukundan, J. Davey, D. Wood, T. Springer, Y. S. Kim, J. Spendelow, T. Rockward, B. Pivovar, M. Arif, D. Jacobson, D. Hussey, K. Chen, K. More, P. Wilde, T. Zawodzinski, V. Gurau, W. Johnson, S. Cleghorn, **Water Transport Exploratory Studies,** Presented at the 2007 DOE EERE Hydrogen, Fuel Cells & Infrastructure Technologies Kick off Meeting, Washington, D.C., Feb. 6–9, 2007.

6. Chen, K. S., "Predicting water-droplet detachment from GDL/channel interfaces in PEM fuel cells", paper accepted for presentation at the 212th ECS Meeting. Manuscript in preparation for publication in the ECS Transaction for the 212th ECS Meeting.

References

1. T. A. Trabold, J. P. Owejan, D. L. Jacobson, M. Arif, and P. R. Huffman, *Int. Journal of Heat and Mass Transfer*, **49**, 4712 (2006).

2. M. A. Hickner, N. P. Siegel, K. S. Chen, D. N. McBrayer, D. S. Hussey, D. L. Jacobson, and M. Arif, *J. Electrochem. Soc.*, **153(5)**, A902 (2006).

3. F. Garzon, Y.S. Kim, R. Mukundan, B. Pivovar, 2006 DOE EERE Hydrogen, Fuel Cells & Infrastructure Technologies Program Review, Arlington, VA, May 18, 2006.

4. Zhang, F. Y.; Yang, X. G.; Wang, C. Y. J. Electrochem. Soc. (2006), 153(2), A225-A232.

5. Theodorakakos, A.; Ous, T.; Gavaises, M.; Nouri, J. M.; Nikolopoulos, N.; Yanagihara, H., J. of Colloid and Interface Science (2006), 300(2), 673-687.